Solution Structure of a Recombinant Type I Sculpin Antifreeze Protein[†,‡]

Ann H.-Y. Kwan,[#] Kayesh Fairley,[#,§] Pia I. Anderberg,[§] Chu Wai Liew,[#] Margaret M. Harding,*[,§] and Joel P. Mackay*[,#]

School of Chemistry and the School of Molecular and Microbial Biosciences, The University of Sydney, NSW 2006, Australia

Received October 17, 2004; Revised Manuscript Received November 21, 2004

ABSTRACT: We have determined the solution structure of rSS3, a recombinant form of the type I shorthorn sculpin antifreeze protein (AFP), at 278 and 268 K. This AFP contains an unusual sequence of N-terminal residues, together with two of the 11-residue repeats that are characteristic of the type I winter flounder AFP. The solution conformation of the N-terminal region of the sculpin AFP has been assumed to be the critical factor that results in recognition of different ice planes by the sculpin and flounder AFPs. At 278 K, the two repeats units (residues 11−20 and 21−32) in rSS3 form a continuous α-helix, with the residues 30−33 in the second repeat somewhat less well defined. Within the N-terminal region, residues 2−6 are well defined and helical and linked to the main helix by a more flexible region comprising residues A7−T11. At 268 K the AFP is overall more helical but retains the apparent hinge region. The helical conformation of the two repeats units is almost identical to the corresponding repeats in the type I winter flounder AFP. We also show that while tetracetylated rSS3 has antifreeze activity comparable to the natural AFP, its overall structure is the same as that of the unacetylated peptide. These data provide some insight into the structural determinants of antifreeze activity and should assist in the development of models that explain the recognition of different ice interfaces by the sculpin and flounder type I AFPs.

The unique properties of AFPs[1] and AFGPs isolated from the blood plasma of fish that inhabit the sub-zero Arctic and Antarctic oceans have attracted enormous interest since their initial discovery by Scholander (*1*) and DeVries (*2*, *3*). Four classes of fish proteins (type I−IV) as well as a single class of glycoprotein have been identified, and the structural characteristics and properties of these AF(G)Ps are summarized in a number of recent reviews (*4*−*6*). These compounds lower the freezing point in a noncolligative manner that results in thermal hysteresis and allow these fish to survive in waters colder than the equilibrium freezing point of their blood and other internal fluids. The ability to suppress ice crystal growth and protect cell membranes from cold-induced damage has led to the application of AF(G)Ps in the food industry, agriculture and medicine (*7*, *8*). However, while significant progress has been made in recent years (*5*, *9*, *10*), the molecular level detail of how each class of AF(G)P is able to inhibit ice growth is still not fully understood. Hence, there are very few reports of de novo design of AF(G)Ps (*11*, *12*) and the tailoring of compounds for specific applications is currently not possible.

The alanine-rich, α-helical type I AFPs have been isolated from the blood serum of the winter (*Pseudopleuronectes americanus*) (*13*) and yellowtail (*Limanda ferruginea*) (*14*) flounders, Alaskan plaice (*Pleuronectes quadritaberulatus*) (*15*), and the grubby (*Myoxocephalus aenaeus*) (*16*), shorthorn (*17*), and Arctic shorthorn (*18*) (*Myoxocephalus scorpius*) sculpins. The most well studied type I AFP is the 37-residue α-helical protein HPLC6 (Figure 1c) (*19*), which accumulates specifically at the {2 0 $\bar{2}$ 1} ice plane (Figure 1) (*15*). While early studies proposed ice growth inhibition mechanisms involving hydrogen bonding to the four Thr residues (*15*, *20*−*22*) that are aligned along one face of the helix (*23*), more recent structure−activity experiments (*24*−*29*) and computational studies (*30*) have identified hydrophobic interactions as a major requirement for activity. From our own studies on synthetic analogues of HPLC6 (*24*−*26*), we proposed that all type I AFPs, including the sculpin AFPs, contain a common hydrophobic face, which is oriented toward the ice surface in the ice/water interface, resulting in inhibition of ice growth (*24*).

In contrast to the type I flounder AFPs, the sculpin AFPs contain a unique N-terminal region (Figure 1b) and accumulate specifically at the {2 $\bar{1}$ $\bar{1}$ 0} plane (Figure 1) (*15*, *31*). While insertion of charged side chains into the ice lattice was proposed to explain this interaction (*31*), recent structure−

[†] This work was supported by an Australian Research Council Discovery Grant.

[‡] The family of 20 low-energy structures at 278 and 268 K (accession codes 1Y03 and 1Y04) has been deposited in the Protein Data Bank. Chemical shift and restraint lists that were used in the structure calculations have been deposited in BioMagResBank (accession code 6427).

* Corresponding authors. Phone: +61293512745/3906. Fax: +61293516650/4726. E-mail: j.mackay@mmb.usyd.edu.au; harding@chem.usyd.edu.au.

[#] School of Chemistry.

[§] School of Molecular and Microbial Biosciences.

[1] Abbreviations: AFP, antifreeze protein; AFGP, antifreeze glycoprotein; CD, circular dichroism; HNHA, three-dimensional heteronuclear (^{1}H-^{15}N-^{1}H) shift correlation double resonance; HPLC, high performance liquid chromatography; NMR, nuclear magnetic resonance; NOE, nuclear Overhauser effect; RDC, residual dipolar coupling; RMSD, residual mean square deviation; SS, shorthorn sculpin; TALOS, torsion angle likelihood obtained from shift and sequence similarity; TOCSY, total correlation spectroscopy; NOESY, nuclear Overhauser effect spectroscopy; DQF−COSY, double quantum filtered correlation spectroscopy; WATERGATE, water suppresssion by gradient tailored excitation.

10.1021/bi047782j CCC: $30.25
Published on Web 01/20/2005

```
                1             11            22
A   rSS3      GS MNAPARAAAK  TAADALAAAKK  TAADAAAAAAA
 4Ac-rSS3  AcGS MNAPARAAAK  TAADALAAAKK  TAADAAAAAAA
                          *            **
B   SS3         XMNAPARAAAK  TAADALAAAKK  TAADAAAAAAAA
    GS5         XMDAPAIAAAK  TAADALAAAKK  TAADAADAAAAA  AKP

    SS8       AcMDGETPAQKAARLAAAAAALAAK  TAADAAAKAAAI AAAAASA
    GS8         XMDGETPAQKAARLAAAAAALAAK  TAADAAAKAAAI AAAAA

C   HPLC6   D TASDAAAAAAL  TAANAKAAAEL  TAANAAAAAAA TAR
    HPLC8   D TASDAAAAAAL  TAANAKAAAKL  TADNAAAAAAA TAR
    YTP     D TASDAAAAAAA  TAAAAAKAAAD  TAAAAAKAAAD TAAAAAEAAAATAR
    AP      D TASDAAAAAAA  TAAAAKAAAEK  TARDAAAAAAA TAAAAR
                repeat 1      repeat 2      repeat 3
```

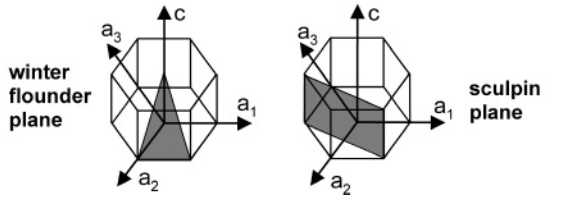

FIGURE 1: Amino acid sequences of selected type I AFPS highlighting the 11-residue repeat units present in all sequences and schematic of the hexagonal unit of ice crystal showing the {2 0 $\bar{2}$ 1} or winter flounder ice plane and the {2 $\bar{1}$ $\bar{1}$ 0} or the sculpin plane. (A) Recombinant SS3 (rSS3) and the acetylated derivative 4Ac-rSS3. The additional GS residues at the N-terminus are numbered −1, −2 to allow comparison with the other type I AFPs shown. Acetylated lysine side chains in 4Ac-rSS3 are marked with an asterisk. (B) Type I sculpin AFPs from the shorthorn (SS) and grubby (GS) sculpins subdivided by length and homology of the first 11 residues. X indicates a blocking group in each sequence which is assumed to be Ac, on the basis of the resequencing of SS8 (*30*), where this group was identified. (C) Type I flounder sequences from the winter flounder (HPLC), yellowtail flounder (YF), and Alaskan plaice (AP).

activity studies (*32*) have ruled out this mechanism and confirmed that, as in the case of the type I flounder AFPs, the hydrophobic face of shorthorn sculpin AFPs is required for antifreeze activity. The structure of the N-terminal residues in the sculpin AFPs also has a direct impact on inhibition properties, and both the naturally occurring fish sequences (*17*, *32*) and a recombinant form of a sculpin AFP reported by our group (*33*) require an *N*-acetyl blocking group for hysteresis.

The outstanding question is why the structurally related type I AFPs recognize different ice planes (Figure 1). Two hypotheses have been put forward in the literature. First, computational studies have shown that there is significant charge inhomogeneity at the ice/water interface (*34*) and hence recognition of different ice planes by the flounder and sculpin sequences may be related to the overall charge/ dipole of the different peptides (*33*). This proposed role of charge/ dipole in the mechanism is consistent with the observations that blocking of the N-terminus in the sculpin AFP increases hysteresis (*17*). The alternate structural hypothesis is based on the conformation of the N-terminal residues from modeling studies, which proposed that steric matching results in folding of the N-terminal residues away from the surface and directs the rest of the sequence to a specific ice plane (*32*). In both hypotheses, the exact role of the N-terminal region of the sculpin AFPs is unclear, particularly in the absence of an NMR or X-ray structure of any of the sculpin sequences.

In this paper we report the solution structure of a recombinant form of the shorthorn sculpin SS3 (rSS3, Figure 1a) and the effects of tetraacetylation on the structure of rSS3. These studies were made possible by uniform labeling of the rSS3 with both ^{15}N and ^{13}C, and the structures are compared at 5 and −5 °C. In particular, the conformation of the N-terminal region, the effect of the *N*-acetyl groups, and how these residues influence the conformation of the rest of the chain have been assessed. This solution data is essential for molecular simulations of the interaction of the sculpin AFPs with the ice/water interface in order to develop models that explain the selective interaction of the AFP with the {2 $\bar{1}$ $\bar{1}$ 0} ice plane, and hence assist in the rational design of synthetic AFPs.

EXPERIMENTAL PROCEDURES

Cloning, Overexpression, and Purification of rSS3. Proteins were overexpressed and purified as previously described (*33*) except for the following. For the production of ^{13}C,^{15}N-labeled rSS3, large-scale overexpression was carried out in a New Brunswick Scientific Bioflow III Fermentor using the protocol of Cai et al. (*35*) Three-liter cultures were grown in a minimal media, in which the only source of nitrogen and carbon were $^{15}NH_4Cl$ and limiting amounts of glucose, respectively. When the dissolved oxygen content increased sharply (indicating exhaustion of glucose), 1.5 g and subsequently 22.5 g of ^{13}C-glucose was added to the culture. All subsequent overexpression and purification procedures were carried out as described previously (*33*) to give protein that was >99% pure by integration of the HPLC trace. rSS3 is used throughout the remainder of the text to refer to ^{13}C,^{15}N-labeled rSS3.

Acetylation Procedure. rSS3 (0.8 mg) was dissolved in water (25 μL), sodium acetate (saturated, 25 μL) was added, and the solution was cooled to 0 °C. Acetic anhydride (5 × 1 μL) was added over 2 h at 0 °C. The reaction was stirred, centrifuged and allowed to stand at 0 °C for an additional 4 h. The reaction was diluted to 400 μL with the HPLC solvent system and purified by reverse phase HPLC (0.05% TFA in 20−60% aqueous acetonitrile over 100 min at 2.5 mL per min on a semipreparative Jones wide pore column. 4Ac-rSS3 was obtained as a white solid in >99% purity by integration of the HPLC trace; ESI MS 3414.5 ($M+H^+$, 80%), 1718.3 ($[M+H+Na]^{2+}$, 100).

NMR Spectroscopy. Samples were prepared for NMR spectroscopy as described previously (*33*). Experiments were carried out at 278 and 268 K on a 600-MHz Bruker DRX600 spectrometer. Water suppression was achieved using pulsed-field gradients and the WATERGATE sequence (*36*). The following homonuclear 2D spectra were recorded on the rSS3 sample: DQFCOSY (*37*), TOCSY (*38*) (τ_m = 35 and 70 ms) and NOESY (*39*) (τ_m = 50 and 150 ms). Acquisition times were 33 and 131 ms for each of these experiments in t_1 and t_2, respectively.

Backbone ^{1}H, ^{15}N, and ^{13}C resonances were assigned using a combination of standard triple resonance experiments as described previously (*40*). Spectra were processed using XWINNMR (Bruker) and analyzed using either XEASY (*41*) or SPARKY (*42*).

^{15}N T_1,T_2 and NOE values were measured on [^{15}N,^{13}C]-rSS3 using the Bruker pulse programs hsqct1etf3gpsi and hsqct2etf3gpsi, respectively. Relaxation delays of 0.01, 0.2, 0.4, 0.7, 0.9, 1.1, 1.3, 1.8, 2.0 and 3.0 s were used in the T_1 experiment, while values of 0.0172, 0.086, 0.1548, 0.2236, 0.2924, 0.3612, 0.430, 0.4988, 0.5676, 0.6364 were used to

measure T_2 values. Recycle delays of 5 s were used in both experiments. Peaks were integrated and T_1 and T_2 data fitted to two-parameter exponentials using a module within SPARKY.

Structure Calculations. Structure calculations for rSS3 at 278 and 268 K were carried out as previously described (*40*, *43*). Standard NOE distance restraints as well as dihedral angle restraints derived from a 3D HNHA (*44*) and TALOS (*45*) were incorporated into structure calculations using the package ARIA1.2 (*46*). For the 278 K structures, RDCs were measured as described previously (*33*) and incorporated into structure calculations in the standard manner in ARIA1.2. The magnitudes of the axial and rhombic components of the alignment tensor were estimated from the average values for the 10 lowest-energy structures (calculated without RDC constraints) using the program SSIA (*47*). No hydrogen bond restraints were used in the structure calculations. Overall, two nonsequential interresidue NOEs for which no consistent assignment could be determined were excluded from the final calculations. Finally, the 100 lowest-energy structures were refined in a 9 Å shell of water molecules (*48*). The 20 conformers with the lowest value of E_{tot} were visualized and analyzed using the programs MOLMOL (*49*) and PROCHECK (*50*).

RESULTS

Structure Calculations. In common with all type I AFPs, the amino acid sequence of rSS3 contains a very high proportion of alanine (25 out of 33 residues), and the structure is primarily helical. As a consequence, severe overlap is observed in NMR spectra of the AFP. To circumvent this problem, we created a recombinant expression system for SS3 (*33*) and overexpressed and purified uniformly ^{13}C,^{15}N-labeled rSS3. The additional dispersion available from the ^{15}N and ^{13}C chemical shift ranges in the labeled protein allowed full resonance assignment of overlapping signals in the ^{1}H spectrum.

A standard set of triple resonance and homonuclear NMR experiments allowed assignment of all backbone ^{1}H, ^{15}N and ^{13}C resonances at 278 K. A combination of backbone ϕ and ψ dihedral angle restraints from the program TALOS and NOE data, supplemented by ^{1}H-^{15}N dipolar coupling measurements (Figure 2), allowed determination of the full solution structure of rSS3 using ARIA1.2. Due to the large number of alanine residues, the ability of ARIA to incorporate ambiguous distance restraints was very valuable. The 20 lowest-energy structures from the final ARIA calculations were chosen to represent the solution structure of rSS3 (Figure 3A) and structural statistics for the ensemble are given in Table 1.

The Overall Three-Dimensional Structure of rSS3. The structure of rSS3 is highly α-helical (Figures 2,3), consistent with our preliminary data (*33*). The main portion of the helix is straight; the measured residual dipolar couplings provide confidence in this conclusion. Overall, the primary structure comprises three sections−a unique N-terminal region and two 11-residue repeats typical of type I AFPs (Figure 3B). The two repeats units (residues 11−20 and 21−32) are very well defined (with an RMSD of 0.33 ± 0.09 Å over residues 12−29) and form an essentially ideal α-helix. The corresponding residues from the two repeats are thus aligned on

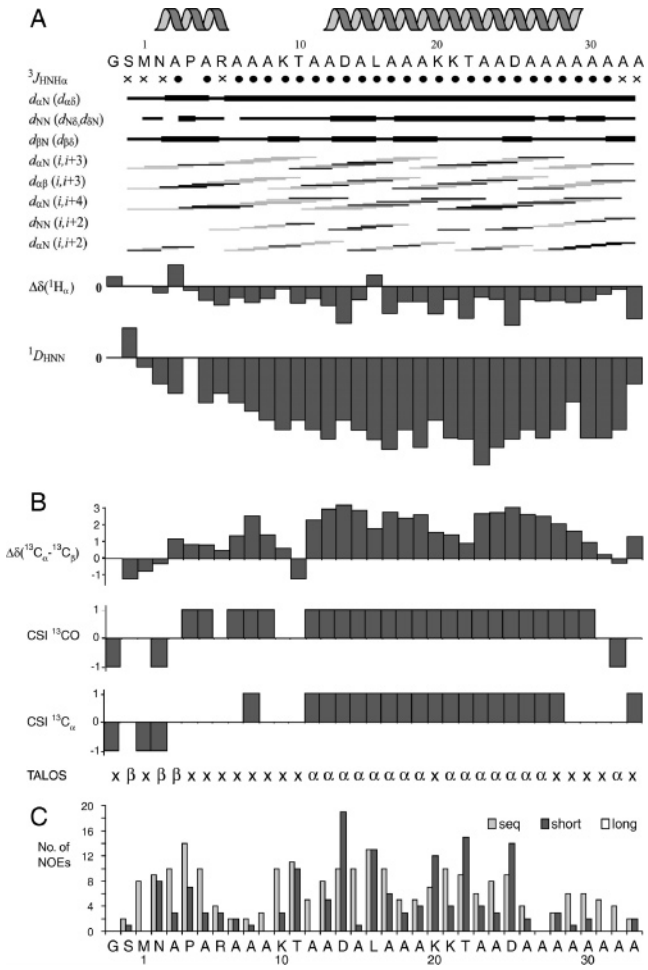

FIGURE 2: Summary of NMR data acquired for rSS3 at 278 K. Residues identified as helical in the final structure are indicated at the top. (A) NOE, *J*-coupling, and residual dipolar coupling data ($^{1}D_{HNN}$) taken from Fairley et al (*33*). Filled circles indicate $^{3}J_{HNH\alpha} < 6.0$ Hz, while crosses indicate $^{3}J_{HNH\alpha} = 6.0-8.0$ Hz. Thin and thick bars indicate strong and weak NOE intensity, respectively. Overlapped NOEs are identified by a light gray line. $^{1}H_\alpha$ chemical shift changes relative to random coil values are shown; negative values are indicative of a helical conformation. (B) ^{13}C chemical shift data. $\Delta\delta(C_\alpha - C_\beta)$ provides an indication of secondary structure; positive values indicate α-helix, while negative values indicate β-sheet. The chemical shift indices for $^{13}C'$ and $^{13}C_\alpha$ are also shown; values of +1 indicate α-helix and −1 indicate β-sheet. (C) Numbers of short- and medium-range NOEs used in the structure calculations.

one face of the helix. The C-terminal part of the second repeat (residue 30−33) is less well defined, yet shows indications of nascent α-helical structure; the ϕ and ψ angles adopted by these residues still tend to fall into the helical region of the Ramachandran plot. Residues 2−6 (the first part of the atypical N-terminal region) are also well defined and quite helical (backbone RMSD of 0.21 ± 0.09 Å). However, this region is generally recognized as 3_{10} helix by the DSSP algorithm implemented in MOLMOL (9 out of 20, with another 1 recognized as α-helix). The remaining structures appear to be helical by manual inspection and from the Ramachandran plot but are not recognized by MOLMOL as helical. Interestingly, the orientation of this region is poorly defined relative to the central repeats.

Conformation of N-Terminal Region. To ascertain whether the apparent mobility of the N-terminal region is real, a number of measured NMR parameters were examined. Residues A7, A8, and A9 were substantially overlapped in

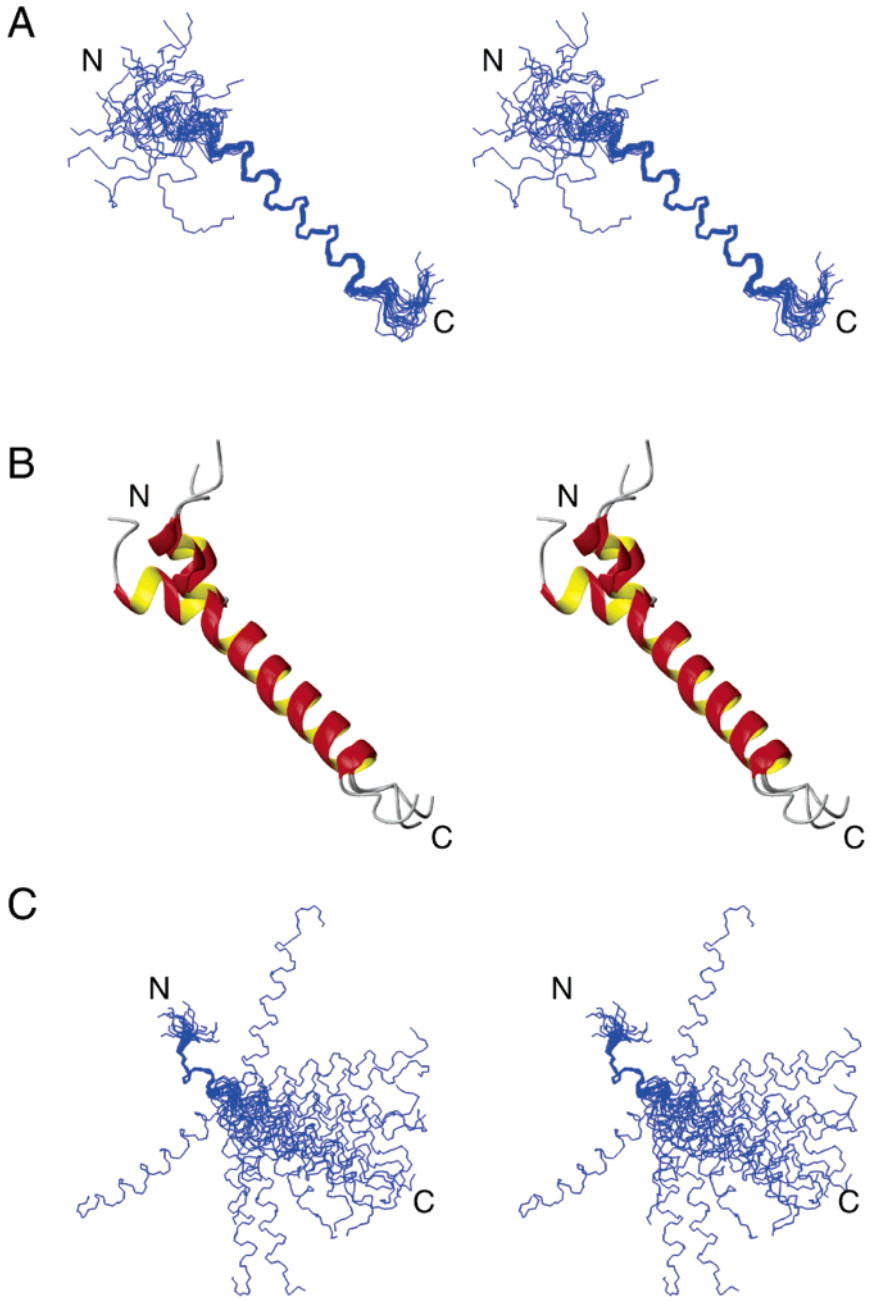

FIGURE 3: Solution structure of rSS3 determined at 278 K. (A) Ensemble of the 20 lowest-energy models of rSS3. Structures are superimposed over the backbone atoms (C_α, C′, N) of residues 11−27. (B) Superimposition of ribbon diagram of the three lowest-energy models of rSS3, showing elements of secondary structure as recognized in the program MOLMOL. (C) Superimposition of the 20 conformers from A, over the backbone atoms of residues 2−6. All structures are shown as wall-eyed stereo images.

all dimensions, and it is possible that this precluded the identification of a number of NOEs; the total number of assigned NOEs for these residues was relatively low (Figure 2) and the backbone in this region is poorly ordered (angle order parameters < 0.7 for backbone ϕ and ψ angles). ^{13}C Chemical shifts do indicate some α-helical propensity (Figure 2) but somewhat less than the two repeats (as judged for example by the magnitude of the $C_\alpha - C_\beta$ shift difference).

^{15}N relaxation parameters (T_1, T_2, and $\{^1H,^{15}N\}$-NOE) were also measured for each residue (Figure 4). These data indicate that the protein is most highly ordered in the region T11-A30, with a gradual drop-off toward the two termini. Thus, no significant additional motion was observed for residues in the A7−T11 region. In combination, these data indicate that while residues A7−T11 may be slightly more flexible than the surrounding sequence, this effect is probably magnified in the NMR structure due to the lack of NOEs for residues A7−A9.

Effect of Temperature on Structures. The effect of temperature on structure was assessed by determination of the structure of rSS3 at 268 K. By reducing the temperature of the NMR sample very slowly (0.2 °C every 10 min), sample freezing was prevented, and a full series of NMR experiments was recorded in this supercooled state.

These data were analyzed independently of the 278 K data, and although the spectra were poorer overall as a consequence of the increased viscosity, sufficient NOE and dihedral angle restraints (from an HNHA together with TALOS; Figure 5) were obtained to allow the structure of rSS3 to be determined. Structural statistics are given in Table

Table 1: Structural Statistics for rSS3

		278 K	268 K
Experimental Input			
total NOE restraints		455	483
total unambiguous restraints		437	452
intraresidue		245	266
sequential		115	128
medium range (2-4 residues)		77	58
long range (> 5 residues)		0	0
total ambiguous restraints		18	31
total residual dipolar coupling restraints		18	0
torsion angle constraints			
dihedrals f		23	27
dihedrals y		22	25
dihedrals χ_1		0	0
	Quality Control		
PROCHECK statistics	residues in most favored regions	97.8%	98.6%
(for residues 2-29)	residues in allowed regions	2.2%	1.4%
	residues in generou sly allowed regions	0.0%	0.0%
	residues in disallow ed regions	0.0%	0.0%
	RMSD of Backbone Atoms		
12-29		0.33 ± 0.09	0.85 ± 0.39
2-6		0.21 ± 0.09	0.35 ± 0.11
	RMSD of all Heavy Atoms		
12-29		0.62 ± 0.10	1.10 ± 0.35
2-6		0.81 ± 0.18	1.06 ± 0.20
	Mean Deviations from Ideal Geometry		
bond lengths		0.0031 ± 0.0002 Å	0.0027 ± 0.0002 Å
bond angles		$0.40 \pm 0.02°$	$0.35 \pm 0.02°$

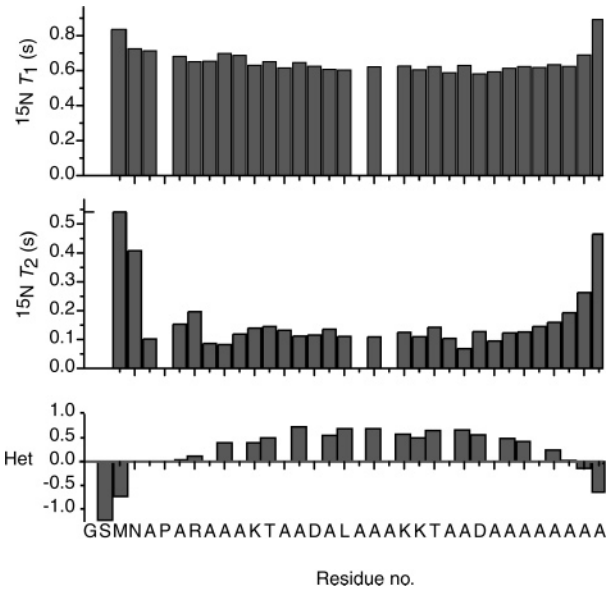

FIGURE 4: Plots of ^{15}N T_1 (upper), T_2 (middle), and $\{^1H\}^{15}N$ heteronuclear NOE (lower) vs residue for rSS3. Data were recorded at 278 K.

1 and the 20 lowest-energy structures from ARIA 1.2 are shown in Figure 6. Note that residual dipolar couplings could not be measured at 268 K due to technical difficulties with the alignment media (bicelles (*51*), filamentous phage (*52*) and acrylamide gels (*53*) were tested).

The structure is extremely similar to that determined at 278 K, although somewhat less well ordered (RMSD of 0.85 ± 0.39 Å over residues 12−29). A "hinge" region between A7 and T11 is still observed in the ensemble, although the data indicate that these residues spend a substantial portion of their time in a helical conformation. The chemical shift data (Figure 5) clearly demonstrate that the protein is more helical at the lower temperature; the central helix extends

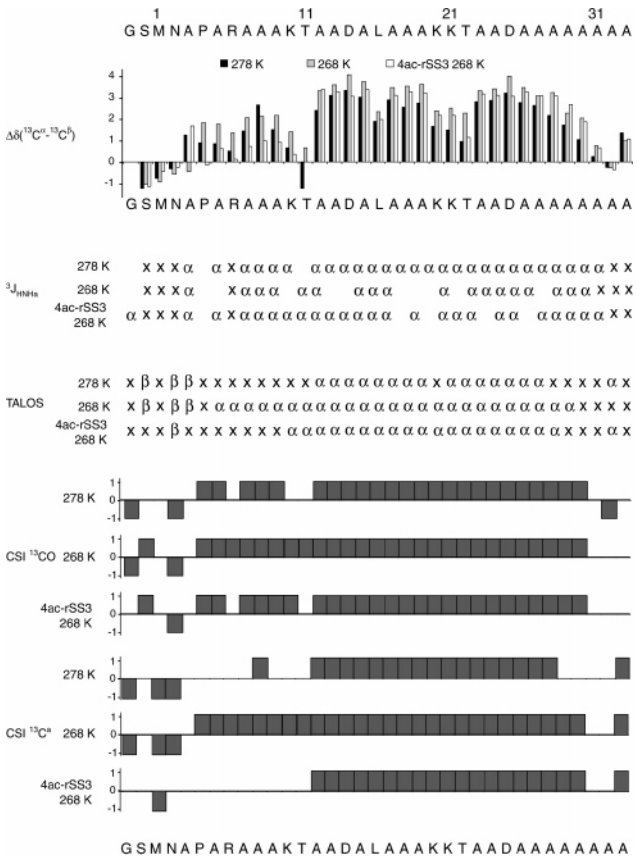

FIGURE 5: Comparison of NMR parameters for rSS3 and 4Ac-rSS3, derived from spectra recorded at 278 and 268 K. Carbon chemical shift, $^3J_{HNH\alpha}$, TALOS, and carbon chemical shift data are shown. Below the amino acid sequence, difference between the C_α and C_β chemical shifts provides an indication of secondary structure for rSS3 at 278 and 268 K and 4Ac-rSS3 at 268 K. $^3J_{HNH\alpha}$ and TALOS prediction are shown below; α represents α-helix, x indicates no prediction, and blanks indicate values could not be measured due to overlap. Chemical shift indices of $^{13}C'$ and $^{13}C_\alpha$ nuclei are also shown.

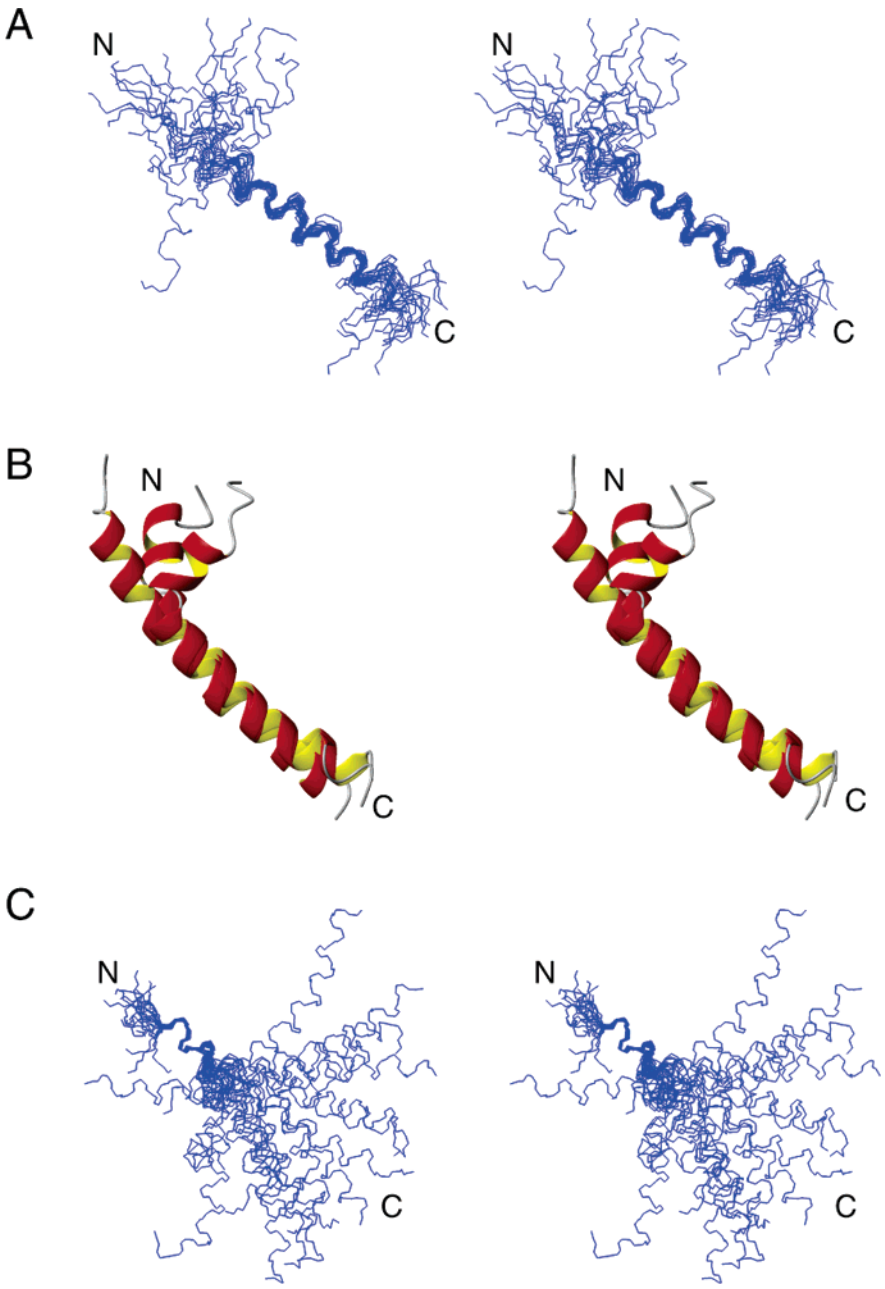

FIGURE 6: Solution structure of rSS3 determined at 268 K. (A) Ensemble of the 20 lowest-energy models. Structures are superimposed over the backbone atoms (C_α, C′, N) of residues 11−27. (B) Superimposition of ribbon diagram of the three lowest-energy models of rSS3, showing elements of secondary structure as recognized in the program MOLMOL. (C) Superimposition of the 20 conformers from A, over the backbone atoms of residues 2−6. All structures are shown as wall-eyed stereo images.

further in both the N- and C-terminal directions compared with the structure at 278 K. However, the amount of helicity does not correlate with the tightness of the structural ensemble, presumably as a consequence of the reduced spectral quality at 268 K and the lack of residual dipolar coupling data. Thus, while the individual models in the ensemble overlay less well with each other at 268 K, residues 2−6 for example are more often helical (19 out of 20 structures at 268 K are predicted to be helical, whereas only 10 out of 20 are predicted to be helical at 278 K).

Figure 7 compares the rSS3 structures at 268 and 278 K. The RMSDs of the backbone atoms for the lowest-energy structure at the two temperatures are 1.08 Å (residues 12−29) and 0.44 Å (residues 4−8). For comparison, the two lowest-energy structures at 268 K have RMSDs of 1.03 Å (residues 12−29) and 0.73 Å (residues 4−8) while the two lowest-energy structures at 278 K had RMSDs of 0.39 Å (residues 12−29) and 0.21 Å (residues 4−8).

Effect of Acetylation on Conformation. We have previously shown that the tetraacetylated derivative 4Ac-rSS3 exhibits significant thermal hysteresis compared with rSS3 (*33*). The increase in thermal hysteresis may be a result of the *N*-acetyl group, the acetylated Lys residues, or a combination of these structural modifications. To ascertain whether this difference in activity was caused by a structural change, the backbone and C_β resonances of 4Ac-rSS3 at 268 K were assigned and $^3J_{HNH\alpha}$ values were measured in an HNHA. Figure 5 summarizes these data and shows that 4Ac-rSS3 is clearly

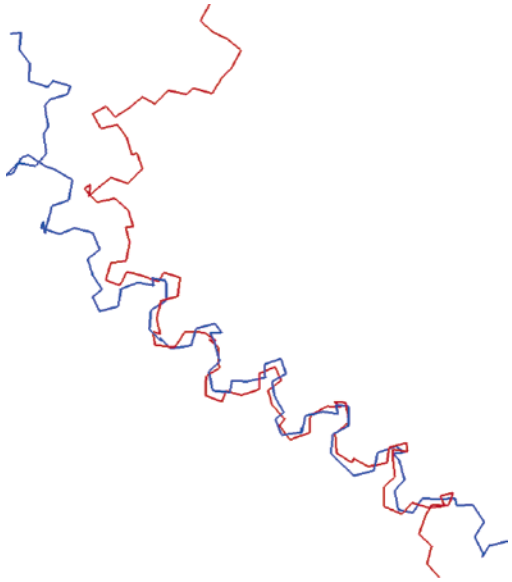

FIGURE 7: Comparison of the lowest-energy structure of rSS3 at 268 (dark line) vs 278 K (light line). The structures are superimposed over the backbone atoms of residues 12−29.

also highly helical. However, it appears that the degree of helicity present in 4Ac-rSS3 is intermediate between that displayed by rSS3 at 278 and 268 K.

DISCUSSION

Understanding the origin of the unique recognition properties of the flounder and sculpin type I AFPs is an important goal in establishing the mechanism of action of antifreeze proteins. Recent advances in understanding of the nature of the ice/water interface (*54*, *55*) have allowed, for the first time, calculations of the hydrogen bonding between the flounder AFP, HPLC6, in water and the dynamic ice−water interfacial region (*30*). These studies have used the crystal structure of HPLC6 (*23*) as a starting point in simulations and have confirmed experimental results that have identified hydrophobicity, not hydrogen bonding, as the key interaction required for antifreeze actvity (*24*−*29*).

In contrast to the flounder type I AFPs, there is comparatively little data available on the sculpin AFPs. The clear distinguishing feature between these two type I subclasses (Figure 1b,c), is the composition of the first 11 N-terminal residues (labeled repeat 1 in Figure 1), and this has led to speculation on the role of this region of the AFP in the mechanism of ice growth inhibition (*15*, *17*, *32*, *33*). In particular, an unusual nonhelical conformation in repeat 1, due to the presence of helix destabilizing residues in the sculpins, has been assumed to the critical difference between the sculpin and flounder AFPs that results in different ice plane recognition. A second important piece of experimental data, unique to the sculpins, is the requirement of an *N*-acetyl group for hysteresis. A structural role in which this N-cap stabilizes the overall helicity of the sculpin AFPs and/or leads to an unusual conformation of the N-terminal residues has also been suggested to be important for antifreeze activity (*5*, *17*, *31*, *32*).

The NMR structure of rSS3 reported in this paper is the first solution structure of a type I sculpin AFP. Determination of the full structure of the AFP is an essential prerequisite to development of a hypothesis to explain the experimental ice growth inhibition properties, including recognition of the $\{2\ \bar{1}\ \bar{1}\ 0\}$ ice plane (Figure 1). As the most relevant conformation(s) adopted by the AFP are those that occur in the fluid ice/water interfacial region, and in the hysteresis gap, the structure of rSS3 has been compared at 278 and 268 K. Previous structural characterization of the native AFP, SS3, has been limited to CD studies (*17*). The incorporation of ^{15}N and ^{13}C labels into rSS3 by recombinant methods has allowed a significant improvement in resonance assignment compared with unlabeled or ^{13}C-labeled samples (*33*), and has thus overcome difficulties in previous NMR studies of both naturally occurring (*56*) and synthetic type I AFPs (*27*, *57*), which have been hampered by poor signal dispersion due to the high number of alanine residues.

Comparison of rSS3 and HPLC6. The repeat units 2 and 3, which are present in both rSS3 and HPLC6, show a high degree of overlap, and in each AFP, the highly helical conformation positions the Thr residues at the start of repeats 1 and 2 along one face of the helix. Comparing the conformation of the residues labeled repeat 1 in rSS3 and HPLC6, the most notable difference between the two structures lies in the hinge region found in rSS3, (A7−T11). A combination of NMR data indicates that motion around this hinge is likely to be rather restricted, although our data are not sufficient to define the likely orientation(s) taken up by this region. Thus, while the N-terminal region of rSS3 is helical overall, despite the presence of the Pro at position 4, the relative orientation of this region with respect to the main portion of the protein is less well defined. Given its position in the primary structure, N2 could potentially act as an N-cap for the N-terminal segment of the helix. However, no evidence for N-capping is apparent from our studies, and indeed the presence of Pro at position 4 reduces the need for such a cap − one less 'free' amide proton exists compared to the N-terminal regions of most helices.

The conformation of repeat 1 in rSS3 contrasts with recent a modeling study of SS8 which proposed that the first 11 residues of SS8 are folded back on the main portion of the helix (*32*). The fold was proposed to be induced by Pro and to be stabilized an unusual capping structure involving several salt bridges and it was suggested, from ice/vacuum modeling, that this conformation directs the rest of the sequence to accumulate at the $\{2\ \bar{1}\ \bar{1}\ 0\}$ plane. It is clear that an analogous structure does not exist for rSS3 and that Pro does not induce a bend in the structure.

Role of the N-Acetyl Blocking Group. The requirement for an *N*-acetyl group for hysteresis in both rSS3 and the natural AFPS, SS3, and SS8 (*17*, *32*) remains an intriguing and unexplained aspect of antifreeze activity in the sculpin AFPs. Even though rSS3 contains an additional two GS residues at the N-terminus due to the expression system used, it does not display thermal hysteresis; in contrast, the tetraacetylated derivative 4Ac-rSS3 exhibits significant hysteresis (0.4 degrees at 15 mg/mL) (*33*). Consistent with this finding, acetylation of SS8 was reported to increase the thermal hysteresis from 0.26 to 0.67 degrees (10 mg/mL) (*17*). In the case of 4Ac-rSS3, the Lys residues are also acetylated, and hence the conformation of this derivative was examined for any significant modifications that may explain its activity.

The NMR data obtained for 4Ac-rSS3 show that the *N*-acetyl group does not have a significant structural effect on the helicity of the polypeptide compared with rSS3. If

anything, 4Ac-rSS3 is slightly less helical than rSS3 at the same temperature. Further, the side chains of Lys10, Lys20, and Lys21 in the rSS3 structures are relatively flexible, indicating that the addition of acetyl groups to these side chains does not result in any significant structural changes in the positions of these side chains. These conclusions are supported by an examination of backbone chemical shifts, which show minimal shift changes between the two samples. Thus, there is no evidence that the *N*-acetyl group induces a structural change that explains the experimental thermal hysteresis data. This conclusion is consistent with the fact that acetylation of rSS3, which has GS at the N-terminus, increases hysteresis by about the same amount as acetylation of SS8 which has MN at the N-terminus. One would not necessarily expect *N*-acetylation to have a similar structural effect on these two sequences due to the different secondary structure preferences and capping effects of GS residues compared with MN residues located at the N-terminus of helices.

Molecular simulations have shown that there are specific and unique charge profiles associated with the various ice/water interfaces (*34*, *54*, *55*), and hence it has been proposed that recognition of the overall charge inhomogeneity may be a significant factor that results in the different ice plane recognition by the sculpins and flounders (*33*, *34*). The lack of a structural change on acetylation lends further support to this hypothesis; conversion of the protonated N-terminus to an *N*-acetyl derivative will influence the overall dipole and charge distribution in the polypeptide, and in particular in the N-terminal region of the sequence.

Role of Helicity. Several AFPs have been shown to maintain their fold at very low temperatures and an increase in α-helical content is observed with a decrease in temperature in other type I AFPs (*58*). While activity levels have been reported to increase with helical content for two homologues of the flounder AFPs (*59*), there is no clear correlation between helicity and activity. For example, highly helical mutants of type I AFPs can show marked decreases in activity (*58*) and specific mutations in skin-type AFP have been shown to increase activity by 15%, while reducing the helical content from 80 to 60% (*59*). The data presented for rSS3 confirm that there is not a simple correlation of this type, and that to some extent the determinants of hysteresis are somewhat more subtle.

CONCLUSION

The NMR structure of rSS3 represents the first complete solution structure of a synthetic type I AFP. This structure is a useful starting point for simulations with the ice/water interface that are required in order to fully understand the molecular level mechanism of ice growth inhibition. The structure shows no evidence for a specific N-terminal conformation that could direct the rest of sequence to a specific ice plane, as has been proposed for SS8 (*32*). The N-blocking acetyl group does not stabilize the helical conformation, nor contribute to an obvious N-capping interaction and hence there is no structural evidence that explains the increase in thermal hysteresis when rSS3 is converted to 4Ac-rSS3. While the helical conformation of the type I AFPs is essential to provide a scaffold that orients the side chains in a specific manner and generates a hydrophobic face, it is clear that overall helicity is not sufficient for activity, and that prediction of antifreeze activity from structure alone is not straightforward.

ACKNOWLEDGMENT

AK is supported by an Australian Postgraduate Award. We thank Dr. W. A. Bubb for expert maintenance of the DRX600 NMR spectrometer at the University of Sydney and Professor A. D. J. Haymet for helpful discussions.

REFERENCES

1. Scholander, P. F., Dam, L. V., Kanwisher, J., Hammel, T., and Gordon, M. S. (1957) Supercooling and Osmoregulation in Arctic Fish, *J. Cell. Comp. Physiol. 49*, 5−24.
2. DeVries, A. L. (1969) Freezing Resistance in some Antarctic Fishes, *Science 163*, 1073−1075.
3. DeVries, A. L., Komatsu, S. K., and Feeney, R. E. (1970) Chemical and Physical Properties of Freezing Point-depressing Glycoproteins from Antarctic Fishes, *J. Biol. Chem. 245*, 2901−2908.
4. Yeh, Y., and Feeney, R. E. (1996) Antifreeze Proteins − Structures and Mechanisms of Function, *Chem. Rev. 96*, 601−617.
5. Harding, M. M., Ward, L. G., and Haymet, A. D. J. (1999) Type I 'antifreeze' proteins − Structure−activity studies and mechanisms of ice growth inhibition, *Eur. J. Biochem. 264*, 653−665.
6. Harding, M. M., Anderberg, P. I., and Haymet, A. D. J. (2003) "Antifreeze" Glycoproteins from Polar Fish, *Eur. J. Biochem. 270*, 1381−1392.
7. Fletcher, G. L., Goddard, S. V., and Wu, Y. L. (1999) Antifreeze proteins and their genes: From basic research to business opportunity, *Chemtech 29*, 17−28.
8. Feeney, R. E., and Yeh, Y. (1998) Antifreeze Proteins: Current Status and Possible Food Uses, *Trends Food Sci. Technol. 9*, 102−106.
9. Fletcher, G. L., Hew, C. L., and Davies, P. L. (2001) Antifreeze proteins of Teleost Fish, *Annu. Rev. Physiol. 63*, 359−390.
10. Madura, J. D., Baran, K., and Wierzbicki, A. (2000) Molecular recognition and binding of thermal hysteresis proteins to ice, *J. Mol. Recog. 13*, 101−113.
11. Kuiper, M. J., Fecondo, J. V., and Wong, M. G. (2002) Rational design of alpha-helical antifreeze peptides, *J. Pept. Res. 59*, 1−8.
12. Wierzbicki, A., Knight, C. A., Rutland, T. J., Miuccio, D. D., Pybus, B. S., and Sikes, C. S. (2000) Structure−Function Relationship in the antifreeze activity of synthetic alanine-lysine antifreeze polypeptides, *Biomacromolecules 1*, 268−274.
13. Duman, J. G., and DeVries, A. L. (1974) Freezing Resistance in Winter Flounder *Pseudopleuronectus americanus*, *Nature 247*, 237−238.
14. Scott, G. K., Davies, P. L., Shears, M. A., and Fletcher, G. L. (1987) Structural Variations in the Alanine-Rich Antifreeze Proteins of the Pleuronectinae, *Eur. J. Biochem. 168*, 629−633.
15. Knight, C. A., Cheng, C.-H. C., and DeVries, A. L. (1991) Adsorption of α-Helical Antifreeze peptides on Specific Ice Crystal Surface Planes, *Biophys. J. 59*, 409−418.
16. Chakrabartty, A., Hew, C. L., Shears, M., and Fletcher, G. (1988) Primary Structures of the Alanine-Rich Antifreeze Polypeptides From Grubby Sculpin, *Myoxocephalus aenaeus*, *Can. J. Zool. 66*, 403−408.
17. Hew, C. L., Joshi, S., Wang, N.-C., Kao, M.-H., and Ananthanarayanan, V. S. (1985) Structures of Shorthorn Sculpin Antifreeze Polypeptides, *Eur. J. Biochem. 151*, 167−172.
18. Yang, D. S. C., Sax, M., Chakrabartty, A., and Hew, C. L. (1988) Crystal Structure of an Antifreeze Polypeptide and Its Mechanistic Implications, *Nature 333*, 232−237.
19. Fourney, R. M., Joshi, S. B., Kao, M. H., and Hew, C. L. (1984) Heterogeneity of Antifreeze Polypeptides from the Newfoundland Winter Flounder, *Pseudopleuronectes americanus*, *Can. J. Zool. 62*, 28−33.
20. Chou, K. C. (1992) Energy-Optimised Structure of Antifreeze Protein and Its Binding Mechanism, *J. Mol. Biol. 223*, 509−517.
21. Wen, D., and Laursen, R. A. (1992) A model for binding of an antifreeze polypeptide to ice, *Biophys. J. 63*, 1659−1662.
22. Lal, M., Clark, A. H., Lips, A., Ruddock, J. N., and White, D. N. J. (1993) Inhibition of Ice Crystal Growth By Preferential Peptide Adsorption − A Molecular Modelling Study, *Faraday Discuss. 95*, 299−306.

23. Sicheri, F., and Yang, D. S. C. (1995) Ice-Binding Structure and Mechanism of an Antifreeze protein from Winter Flounder, *Nature 375*, 427−431.
24. Haymet, A. D. J., Ward, L. G., and Harding, M. M. (1999) Winter flounder "antifreeze" proteins: Synthesis and ice growth inhibition of analogues that probe the relative importance of hydrophobic and hydrogen-bonding interactions, *J. Am. Chem. Soc. 121*, 941−948.
25. Haymet, A. D. J., Ward, L. G., and Harding, M. M. (2001) Hydrophobic Analogues of the Winter Flounder Antifreeze Protein, *FEBS Lett. 491*, 285−288.
26. Haymet, A. D. J., Ward, L. G., Harding, M. M., and Knight, C. A. (1998) Valine Substituted Winter Flounder Antifreeze − Preservation of Ice Growth Hysteresis, *FEBS Lett. 430*, 301−306.
27. Chao, H., Houston, M. E., Hodges, R. S., Kay, C. M., Sykes, B. D., Loewen, M. C., Davies, P. L., and Sönnichsen, F. D. (1997) A Diminished Role For Hydrogen Bonds in Antifreeze Protein Binding to Ice, *Biochemistry 36*, 14652−14660.
28. Baardsnes, J., Kondejewski, L. H., Hodges, R. S., Chao, H., Kay, C., and Davies, P. L. (1999) New ice-binding face for type I antifreeze protein, *FEBS Lett. 463*, 87−91.
29. Zhang, W., and Laursen, R. A. (1998) Structure−function relationships in a type I antifreeze polypeptide − The role of threonine methyl and hydroxyl groups in antifreeze activity, *J. Biol. Chem. 273*, 34806−34812.
30. Dalal, P., Knickelbein, J., Haymet, A. D. J., Sönnichsen, F. D., and Madura, J. D. (2001) Hydrogen bond analysis of Type 1 antifreeze protein in water and the ice/water interface, *PhysChemComm 7*, 1−5.
31. Wierzbicki, A., Taylor, M. S., Knight, C. A., Madura, J. D., Harrington, J. P., and Sikes, C. S. (1996) Analysis of Shorthorn Sculpin Antifreeze Protein Stereospecific Binding to (2−10) Faces of Ice, *Biophys. J. 71*, 8−18.
32. Baardsnes, J., Jelokhani-Niaraki, M., Kondejewski, L. H., Kuiper, M. J., Kay, C. M., Hodges, R. S., and Davies, P. L. (2001) Antifreeze protein from the shorthorn sculpin: Identification of the ice-binding surface, *Protein Sci. 10*, 2566−2576.
33. Fairley, K., Westman, B. J., Pham, L. H., Haymet, A. D. J., Harding, M. M., and Mackay, J. P. (2002) Type I shorthorn sculpin antifreeze protein. Recombinant synthesis, solution conformation, and ice growth inhibition studies, *J. Biol. Chem. 277*, 24073−24080.
34. Bryk, T., and Haymet, A. D. J. (2002) Ice 1h/water interface of the SPC/E model. Molecular dynamics simulations of the equilibrium basal and prism interfaces, *J. Chem. Phys. 117*, 10258−10268.
35. Cai, M., Huang, Y., Sakaguchi, K., Clore, G. M., Gronenborn, A. M., and Craigie, R. (1998) An efficient and cost-effective isotope labeling protocol for proteins expressed in *Escherichia coli*, *J. Biomol. NMR 11*, 97−102.
36. Piotto, M., Saudek, V., and Sklenar, V. (1992) Gradient-tailored excitation for single-quantum NMR spectroscopy of aqueous solutions, *J. Biomol. NMR 2*, 661−665.
37. Piantini, U., Sorensen, O. W., and Ernst, R. R. (1982) Multiple quantum filters for elucidating NMR coupling networks, *J. Am. Chem. Soc. 104*, 6800−6801.
38. Bax, A., and Davis, D. G. (1985) MLEV-17 based two-dimensional homonuclear magnetisation transfer spectroscopy, *J. Magn. Reson. 65*, 355−360.
39. Kumar, A., Ernst, R. R., and Wüthrich, K. (1980) A two-dimensional nuclear Overhauser enhancement (2D nOe) experiment for the elucidation of complete proton−proton cross -relaxation networks in biological macromolecules, *Biochem. Biophys. Res. Commun. 95*, 1−6.
40. Deane, J. E., Visvader, J. E., Mackay, J. P., and Matthews, J. M. (2002) ^{1}H, ^{15}N and ^{13}C assignments of FLIN4, an intramolecular LMO4: ldb1 complex, *J. Biomol. NMR 23*, 165−166.
41. Bartels, C., Xia, T.-H., Billeter, P., Guntert, P., and Wüthrich, K. (1995) The program XEASY for computer-supported NMR spectral analysis of biological macromolecules, *J. Biomol. NMR 5*, 1−10.
42. Goddard, T. D., and Kneller, D. G. (2002), SPARKY 3, University of California, San Francisco, USA.
43. Kwan, A. H., Gell, D. A., Verger, A., Crossley, M., Matthews, J. M., and Mackay, J. P. (2003) Engineering a protein scaffold from a PHD finger, *Structure 11*, 803−813.
44. Bax, A., Vuister, G. W., Grzesiek, S., Delaglio, F., Wang, A. C., Tschudin, R., and Zhu, G. (1994) Measurement of homo- and heteronuclear J couplings from quantitative J correlation, *Methods Enzymol. 239*, 79−105.
45. Cornilescu, G., Delaglio, F., and Bax, A. (1999) Protein backbone angle restraints from searching a database for chemical shift and sequence homology, *J. Biomol. NMR 13*, 289−302.
46. Linge, J. P., O'Donoghue, S. I., and Nilges, M. (2001) Automated assignment of ambiguous nuclear overhauser effects with ARIA, *Methods Enzymol. 339*, 71−90.
47. Zweckstetter, M., and Bax, A. (2002) Evaluation of uncertainty in alignment tensors obtained from dipolar couplings, *J. Biomol. NMR 23*, 127−137.
48. Jorgensen, W. L., Chandrasekhar, J., Madura, J., Impey, R., and Klein, M. (1983) Comparison of simple potential functions for simulating liquid water, *J. Chem. Phys. 79*, 926−935.
49. Koradi, R., Billeter, M., and Wüthrich, K. (1996) MOLMOL: a program for display and analysis of macromolecular structures, *J. Mol. Graph. 14*, 51−5, 29−32.
50. Laskowski, R. A., Rullmannn, J. A., MacArthur, M. W., Kaptein, R., and Thornton, J. M. (1996) AQUA and PROCHECK−NMR: programs for checking the quality of protein structures solved by NMR, *J. Biomol. NMR 8*, 477−486.
51. Tolman, J. R. (2001) Dipolar couplings as a probe of molecular dynamics and structure in solution, *Curr. Opin. Struct. Biol. 11*, 532−439.
52. Hansen, M. R., Mueller, L., and Pardi, A. (1998) Tunable alignment of macromolecules by filamentous phage yields dipolar coupling interactions, *Nat. Struct. Biol. 5*, 1065−1074.
53. Meier, S., Haussinger, D., and Grzesiek, S. (2002) Charged acrylamide copolymer gels as media for weak alignment, *J. Biomol. NMR 24*, 351−356.
54. Hayward, J. A., and Haymet, A. D. J. (2001) The Ice/Water Interface: Molecular Dynamics Simulations of the Basal, Prism and 202bar1 Interfaces of Ice 1h, *J. Chem. Phys. 114*, 3713−3726.
55. Hayward, J. A., and Haymet, A. D. J. (2002) The ice/water interface. Orientational order parameters for the basal, prism, {202bar1} and {21bar1baro} interfaces of ice Ih., *Phys. Chem. Chem. Phys. 4*, 3712−3719.
56. Sönnichsen, F. D., Davies, P. L., and Sykes, B. D. (1998) NMR Structural Studies on Antifreeze Proteins, *Biochem. Cell Biol. 76*, 284−293.
57. Liepinsh, E., Otting, G., Harding, M. M., Ward, L. G., Mackay, J. P., and Haymet, A. D. J. (2002) Solution Structure of a Hydrophobic Analogue of the Winter Flounder Antifreeze Protein, *Eur. J. Biochem. 264*, 1269−1266.
58. Graether, S. P., Slupsky, C. M., Davies, P. L., and Sykes, B. D. (2001) Structure of Type I Antifreeze Protein and Mutants in Supercooled Water, *Biophys. J. 81*, 1677−1683.
59. Low, W. K., Lin, Q., and Hew, C. L. (2003) The role of N and C termini in the antifreeze activity of winter flounder (*Pleuronectes americanus*) antifreeze proteins, *J. Biol. Chem. 278*, 10334−10343.

BI047782J